Low-frequency oscillation analysis of two-stage photovoltaic grid-connected system

Shao, Bingbing; Miao, Zilong; Wang, Liyuan; Meng, Xiaoxiao; Chen, Zhe

The 5th International Conference on Electrical Engineering and Green Energy, CEEGE 2022, 8–11 June, Berlin, Germany

Low-frequency oscillation analysis of two-stage photovoltaic grid-connected system

Bingbing Shao[a],*, Zilong Miao[a], Liyuan Wang[b], Xiaoxiao Meng[a], Zhe Chen[c]

[a] *Anhui Province Key Laboratory of Renewable Energy Utilization and Energy Saving (Hefei University of Technology), Hefei 230009, China*
[b] *State Grid Changfeng County Electric Power Supply Company, Hefei 231131, China*
[c] *Department of Energy Technology, Aalborg University, 9220 Aalborg, Denmark*

Abstract

The low-frequency oscillation (LFO) problem of photovoltaic (PV) grid-connected systems has been a critical concern for safe operation, whereas the impact of dc-side components of PV plants are always ignored and single-stage PV plant is used. This paper performs a comprehensive analysis of the LFOs in the two-stage PV grid-connected system. The complete small-signal model of the two-stage PV system is built. On this basis, the LFO modes and high-frequency oscillation (HFO) modes are calculated and related participating components are determined. Then, the impact of key parameters on the LFO characteristics is investigated with the root locus analysis. The theoretical analysis is verified through PSCAD/EMTDC simulations.
© 2022 The Author(s). Published by Elsevier Ltd. This is an open access article under the CC BY-NC-ND license (http://creativecommons.org/licenses/by-nc-nd/4.0/).

Peer-review under responsibility of the scientific committee of the 5th International Conference on Electrical Engineering and Green Energy, CEEGE, 2022.

Keywords: Two-stage photovoltaic plant; Low-frequency oscillation; High-frequency oscillation; Small-signal model

1. Introduction

To role of renewable energy has been highlighted due to its advantage in reducing carbon emission, and thus the photovoltaic (PV) power is booming in certain countries. However, wide-frequency oscillations in real grid-connected PV plants have been reported in [1]. Meanwhile, a 7 Hz oscillation was observed in a utility-scale plant during transmission line outage [2]. The low frequency oscillation (LFO) in PV grid-connected system may cause the equipment damage or even system shutdown, so the LFOs in PV systems should be analyzed and suitable parameter optimization strategy should be proposed.

The dynamic modeling of PV system directly affects the LFO characteristics. A typical PV plant is composed of dc-side and ac-side components. For the two-stage PV plant, the dc-side includes the PV arrays and dc–dc boost converter, while the dc-side of the single-stage PV plant only contains the PV arrays. In [3], the LFO characteristics

* Corresponding author.
  E-mail address: shaobingbing1223@163.com (B. Shao).

of single-stage PV plant connected to weak ac networks were analyzed with the impedance analysis method. In [4], the impacts of two different dc-side representations on the LFO were examined and compared, and the comparison indicated that the constant voltage model is more accurate. With the describing function method, the low-frequency and high-frequency oscillation (HFO) of the LCL-filtered single-stage PV generators were analyzed [5]. The 5 Hz LFO in a single-stage PV connected to a weak AC grid was observed in [6], and the influence mechanism of phase-locked loop (PLL) control on the LFO stability was revealed. In [7], the small-signal stability of droop control-based PV clusters was analyzed, in which the PV plant has a single-stage structure.

To the authors' best knowledge, much focus has been put on the stability analysis of single-stage PV plants, while the LFO of two-stage PV plants is less concerned. DC-side components of the PV plant are usually neglected in the literature and are modeled simply with an ideal voltage source [8,9]. Compared with the single-stage PV system, the overall control of two-stage PV system is clearer, as two separate controllers are used, one for the dc–dc boost converter, and another one for the dc–ac inverter. Three-phase two-stage PV grid-connected system is popular on the residential level or commercial level, such as the rooftop PV arrays and PV parks [10]. The two-stage PV grid-connected system is still implemented in the projects and related LFO problems should be paid much focus. To fill in the above gaps, this paper focus on the LFO characteristics analysis of the two-stage PV grid-connected system. The complete small-signal of the two-stage PV system is built in Section 2. In Section 3, the LFO characteristics are analyzed with the eigenvalue analysis, and the components participating in high-frequency oscillation modes are also determined. Concluding remarks are given in Section 4.

2. Dynamic model of two-stage photovoltaic grid-connected system

2.1. System and control structure

The two-stage PV grid-connected system is shown in Fig. 1. The system is composed of PV arrays, dc/dc boost converter, dc–ac inverter, LCL filter, and ac grid. A Perturb & Observe maximum power point tracking (MPPT) algorithm is adopted to determine the optimal PV voltage u_{pv_ref}, and then the dc–dc converter controls the dc-link voltage u_{pv} of PV arrays. The dc–ac inverter controls the dc-link voltage u_{dc} and the ac-side reactive power Q_s. The system and control parameters are shown in Table 1.
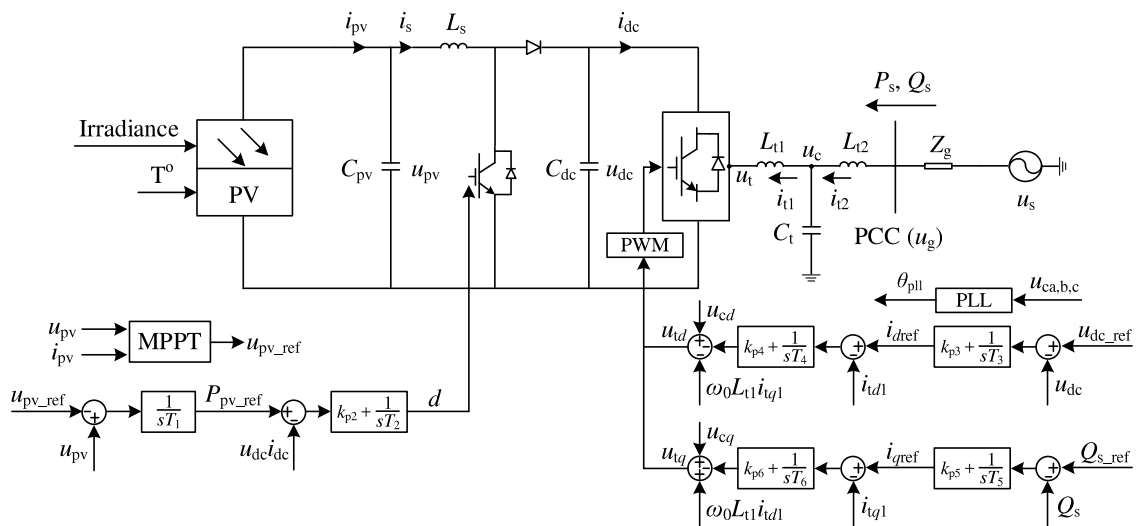

Fig. 1. System and control model of the two-stage PV grid-connected system.

2.2. Small-signal model

As the PV arrays and MPPT mainly affect the steady-state operation points rather than the dynamic characteristics, their modeling is ignored in this paper, and u_{pv_ref} is directly given in Table 1. The dynamic modeling of other modules are shown below.

Table 1. System and control parameters.

Modules	Parameters	Values
dc-side system	Nominated active power	300 kW
	dc-side capacitor ($C_{pv}/\mu F$, $C_{dc}/\mu F$)	1000, 7800
	dc-side inductance ($L_s/\mu H$)	100
ac-side system	LCL filter ($L_{t1}/\mu H$, $C_t/\mu F$, $L_{t2}/\mu H$)	300, 1000, 125
	ac grid impedance and its angle (Z_g/Ω, $\theta_{ac}/°$)	0.2489, 80
dc–dc boost control	u_{pv_ref}/kV	0.132
	T_1, k_{p2}, T_2	0.05, 1, 0.5
dc–ac inverter control	u_{dc_ref}/kV	1
	$Q_{s\_ref}/Mvar$	0
	k_{p3}, T_3	0.5, 0.2
	k_{p4}, T_4	0.15, 0.08
	k_{p5}, T_5	0.3, 0.02
	k_{p6}, T_6	0.15, 0.08
PLL control	k_{p_pll}, k_{i_pll}	9.5, 19

dc–dc boost converter model: The dc–dc converter model includes its circuit model and control model. The dynamic model of its circuit can be represented by (1), assuming always continuous conduction mode operation. Meanwhile, it can be known from Fig. 1 that the dynamic model of its control system is shown in (2).

$$\begin{cases} C_{pv}\dfrac{du_{pv}}{dt} = i_{pv} - i_s \\ L_s\dfrac{di_s}{dt} = u_{pv} - (1-d)u_{dc} \\ C_{dc}\dfrac{du_{dc}}{dt} = (1-d)i_s - i_{dc} = (1-d)i_s + \dfrac{3(u_{td}i_{t1d} + u_{tq}i_{t1q})}{2u_{dc}} \end{cases} \tag{1}$$

$$\begin{cases} \dfrac{dx_1}{dt} = u_{pv} - u_{pv\_ref} \\ \dfrac{dx_2}{dt} = P_{pv\_ref} - u_{dc}i_{dc} = P_{pv\_ref} + 1.5(u_{td}i_{t1d} + u_{tq}i_{t1q}) \end{cases} \tag{2}$$

dc–ac inverter model: The dc–ac inverter model mainly implies its control model. It can be known from Fig. 1 that its dynamic model is shown in (3).

$$\begin{cases} \dfrac{dx_3}{dt} = u_{dc\_ref} - u_{dc}, \dfrac{dx_4}{dt} = i_{dref} - i_{t1d}, i_{dref} = k_{p3}(u_{dc\_ref} - u_{dc}) + \dfrac{x_3}{T_3} \\ \dfrac{dx_5}{dt} = Q_{s\_ref} - Q_s, \dfrac{dx_6}{dt} = i_{qref} - i_{t1q}, i_{qref} = k_{p5}(Q_{s\_ref} - Q_s) + \dfrac{x_5}{T_5} \end{cases} \tag{3}$$

ac-side dynamic model: The ac-side dynamic model implies its circuit model, and it is built in the *x–y* frame, as shown in (4).

$$\begin{cases} L_{t1}\begin{bmatrix}\dfrac{di_{t1x}}{dt} \\ \dfrac{di_{t1y}}{dt}\end{bmatrix} = \begin{bmatrix}u_{cx} \\ u_{cy}\end{bmatrix} - \begin{bmatrix}u_{tx} \\ u_{ty}\end{bmatrix} + \omega_0 L_{t1}\begin{bmatrix}-\dfrac{di_{t1y}}{dt} \\ \dfrac{di_{t1x}}{dt}\end{bmatrix}, C_t\begin{bmatrix}\dfrac{du_{cx}}{dt} \\ \dfrac{du_{cy}}{dt}\end{bmatrix} = \begin{bmatrix}i_{t2x} \\ i_{t2y}\end{bmatrix} - \begin{bmatrix}i_{t1x} \\ i_{t1y}\end{bmatrix} + \omega_0 C_t\begin{bmatrix}-u_{cy} \\ u_{cx}\end{bmatrix} \\ (L_{t2} + L_g)\begin{bmatrix}\dfrac{di_{t2x}}{dt} \\ \dfrac{di_{t2y}}{dt}\end{bmatrix} = \begin{bmatrix}u_{sx} \\ u_{sy}\end{bmatrix} - \begin{bmatrix}u_{cx} \\ u_{cy}\end{bmatrix} - R_g\begin{bmatrix}i_{t2x} \\ i_{t2y}\end{bmatrix} + \omega_0(L_{t2} + L_g)\begin{bmatrix}-i_{t2y} \\ i_{t2x}\end{bmatrix} \end{cases} \tag{4}$$

where $\omega_0 = 120\pi$ is the reference angular frequency. L_g and R_g are the inductance and resistance of the ac grid impedance, respectively.
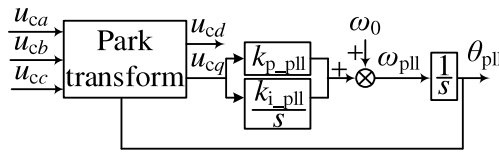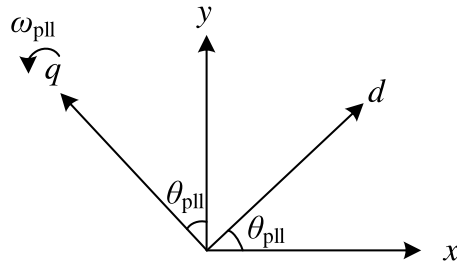
Fig. 2. Control structure of the PLL.

Fig. 3. Relationship between d–q frame and x–y frame.

PLL control model: The detailed control structure of the PLL is shown in Fig. 2, and the dynamic model of the PLL is shown in (5).

$$
\begin{cases}
\dfrac{\mathrm{d}x_{\mathrm{a}}}{\mathrm{d}t} = u_{cq} \\[2mm]
\dfrac{\mathrm{d}x_{\mathrm{b}}}{\mathrm{d}t} = \omega_0 + u_{cq}k_{\mathrm{p\_pll}} + x_{\mathrm{a}}k_{\mathrm{i\_pll}} \\[2mm]
\theta_{\mathrm{pll}} = x_{\mathrm{b}}
\end{cases}
\tag{5}
$$

Interface equation between PV generation system and ac grid: As the control scheme of the two-stage PV generation system and the circuit scheme of the ac grid are established on different frames, an interface transformation equation is required to combine the two different dynamic equations. Fig. 3 shows the relationship between d–q frame and x–y frame, and the interface equation is shown in (6).

$$
\begin{bmatrix} f_x \\ f_y \end{bmatrix} =
\begin{bmatrix} \cos\theta_{\mathrm{pll}} & -\sin\theta_{\mathrm{pll}} \\ \sin\theta_{\mathrm{pll}} & \cos\theta_{\mathrm{pll}} \end{bmatrix}
\begin{bmatrix} f_d \\ f_q \end{bmatrix}
\tag{6}
$$

Small signal model of two-stage PV grid-connected system: Combining (1)–(5), and transforming the dynamic equations in the d–q frame to the x–y frame based on (6), and then linearizing the resultant based on the parameters in Table 1, the small-signal model of two-stage PV grid-connected system is shown in (7).

$$
\frac{\mathrm{d}\Delta\boldsymbol{x}}{\mathrm{d}t} = \boldsymbol{A}\Delta\boldsymbol{x} + \boldsymbol{B}\Delta\boldsymbol{u}
\tag{7}
$$

where $\Delta\boldsymbol{x}$ is the linearized state variables, and $\Delta\boldsymbol{x} = [\Delta u_{\mathrm{pv}}, \Delta i_{\mathrm{s}}, \Delta u_{\mathrm{dc}}, \Delta x_1, \Delta x_2, \Delta x_3, \Delta x_4, \Delta x_5, \Delta x_6, \Delta x_{\mathrm{a}}, \Delta x_{\mathrm{b}}, \Delta i_{\mathrm{t1}x}, \Delta i_{\mathrm{t1}y}, \Delta i_{\mathrm{t2}x}, \Delta i_{\mathrm{t2}y}, \Delta u_{\mathrm{cx}}, \Delta u_{\mathrm{cy}}]$. $\Delta\boldsymbol{u}$ is the linearized input variables, and $\Delta\boldsymbol{u} = [\Delta u_{\mathrm{pv\_ref}}, \Delta u_{\mathrm{dc\_ref}}, \Delta Q_{\mathrm{s\_ref}}]$. $\boldsymbol{A}$ is the linearized state matrix, and $\boldsymbol{B}$ is the linearized input matrix.

3. Oscillation characteristics analysis

3.1. Oscillation modes analysis

Based on the small-signal model of (7), the oscillation modes of the two-stage PV grid-connected system are calculated with the eigenvalue method, as listed in Table 2. Table 2 shows that there are two LFO modes (A1 and A2) and three HFO modes (B1, B2, B3) in the system. The HFO modes present strong damping to the system, whereas the LFO modes present weak damping to the system. Thus, the LFO modes play an important role in the system stability and should be further analyzed.

Table 2. Oscillation modes of two-stage PV grid-connected system.

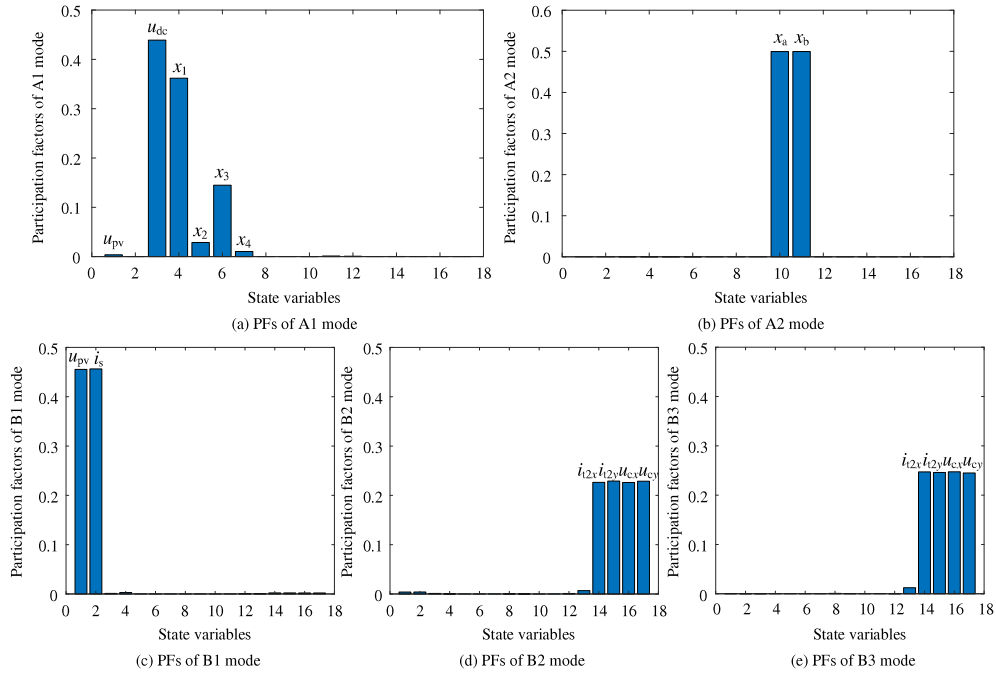| Oscillation modes	Eigenvalues	Frequencies/Hz	Damping ratios
Low-frequency oscillations	A1: $-3.7681 \pm j68.5864$	10.9159	0.0549
	A2: $-4.3264 \pm j50.9734$	8.1127	0.0846
High-frequency oscillations	B1: $-434.53 \pm j3165.7$	503.84	0.1360
	B2: $-479.59 \pm j3205.4$	510.16	0.1480
	B3: $-511.59 \pm j2454.1$	390.58	0.2041

Fig. 4. Participation factors analysis of the oscillation modes.

3.2. Participation factors analysis

The participation factor (PF) is the product of left eigenvectors and right eigenvectors, and it implies the degree to which the state variables participate in the oscillation modes. The PFs of the LFO and HFO modes are calculated, as shown in Fig. 4, where the participating state variables with large participation factors are marked.

PFs analysis of A1 mode: It can be known from Fig. 4(a) that the LFO mode A1 is related to u_{pv}, u_{dc}, x_1, x_2, x_3, and x_4. With these variables' meaning in (2)–(3), the LFO mode A1 is greatly affected by the dc voltage control of the dc–dc boost converter and dc–ac inverter.

PFs analysis of A2 mode: It can be known from Fig. 4(b) that the LFO mode A2 is related to x_a, x_b. With these variables' meaning in (5), the LFO mode A2 is greatly affected by the PLL control.

PFs analysis of B1 mode: It can be known from Fig. 4(c) that the HFO mode B1 is related to u_{pv}, i_s. Thus, the HFO mode B1 mainly results from the LC resonance in the dc-side system.

PFs analysis of B2, B3 modes: It can be known from Fig. 4(d) and (e) that the HFO modes B2 and B3 are related to i_{t2x}, i_{t2y}, u_{cx}, u_{cy}. Thus, the HFO modes B2 and B3 mainly result from the LC or LCL resonance in the ac-side system.

The above analysis indicates that the dc–dc boost converter and the dc voltage control of dc–ac inverter greatly affect the LFO modes of the two-stage PV system. Assuming a constant dc-side voltage and ignoring the dynamics of PLL [8,9] will make the two LFO modes disappear, which can result in misleading stability analysis conclusions. Ignoring the dynamics of dc–dc boost converter [4] will affect the value of LFO mode A1.
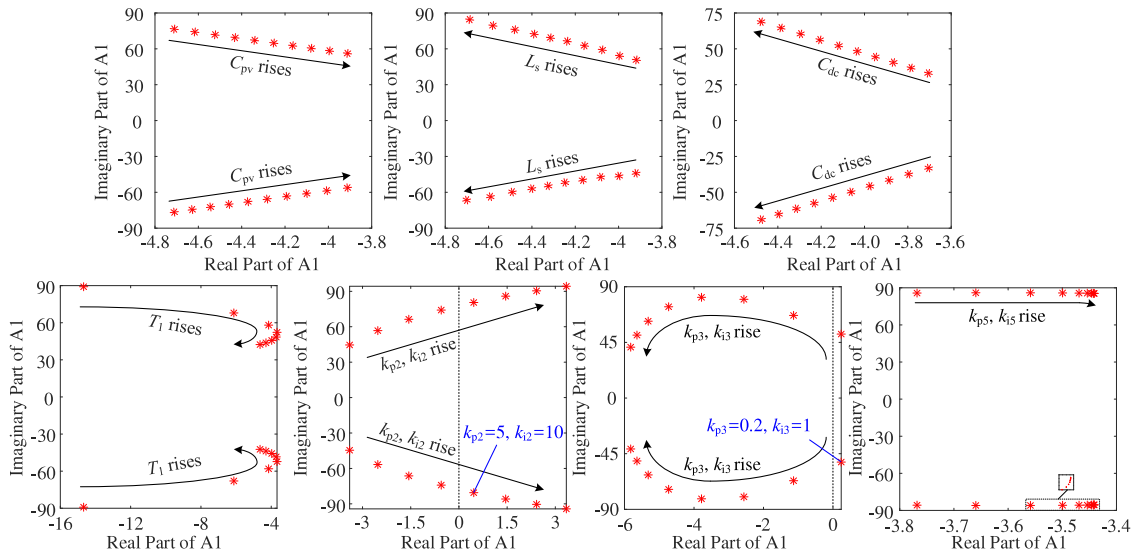
(a) The impact of dc-dc boost converter and dc-ac inverter parameters on the LFO mode A1
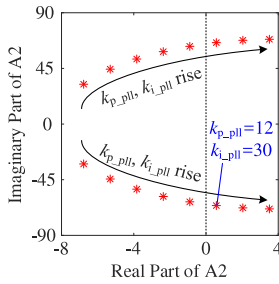
(b) The impact of PLL control on the LFO mode A2
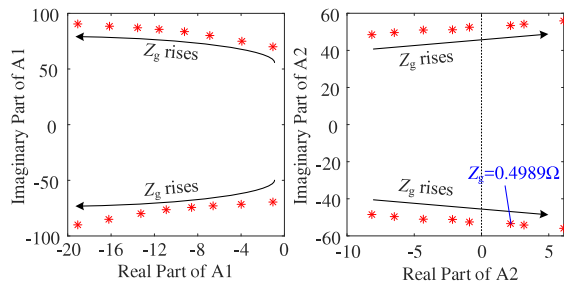
(c) The impact of grid impedance on the LFO modes A1 and A2

Fig. 5. The impact of various parameters on the LFO modes A1 and A2.

3.3. Root locus analysis

The impact of critical system and control parameters on the LFO modes A1 and A2 is analyzed with the root locus analysis, as shown in Fig. 5. The proportional coefficient and integral coefficient in PI controllers change at a fixed proportion at the same time.

Fig. 5(a) shows that with the increase of C_{pv}, inner control gain of the dc–dc converter and dc–ac inverter, the damping of the LFO mode A1 decreases. On the contrary, with the increase of L_s, C_{dc}, outer control gain of the dc–ac inverter, the damping of the LFO mode A1 increases. Especially, with the increase of T_1, the damping of the LFO mode A1 decreases first and then increases. Besides, large inner control gains of the dc–dc converter and small outer control gains of the dc–ac inverter can trigger the instability of LFO mode A1.

Fig. 5(b) shows that with the increase of the PLL control gain, the damping of the LFO mode A2 decreases. Excessive PLL control gain can result in the instability of LFO mode A2.

Especially, Fig. 5(c) shows that the grid strength has a different impact on the LFO modes A1 and A2. The increase of grid impedance can suppress the LFO mode A1, whereas the increase of grid impedance degrades the LFO mode A2. Excessive grid impedance can result in the instability of LFO mode A2.

3.4. PSCAD/EMTDC simulation verification

The simulation model of Fig. 1 is built in the PSCAD/EMTDC, and the parameters are shown in Table 1. The parameters are adjusted to improper values at 3 s to verify the instability phenomenon of Fig. 5, as shown in Fig. 6.
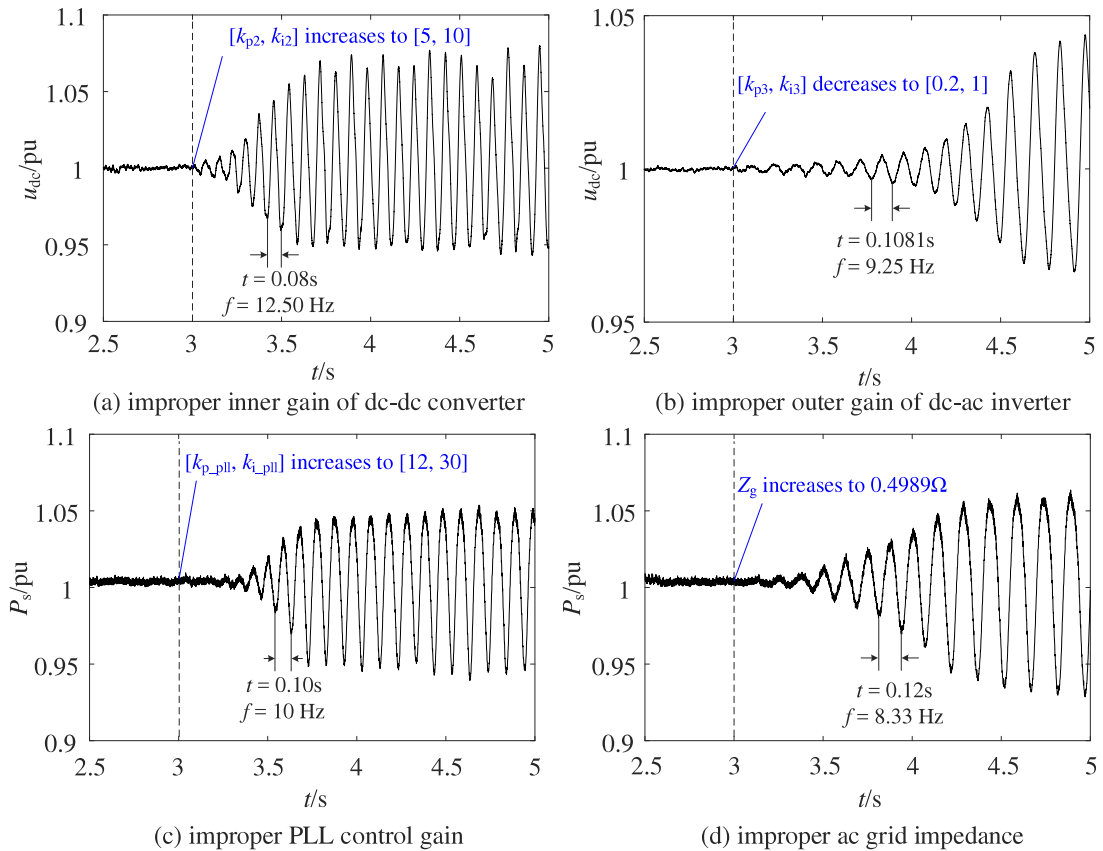
Fig. 6. PSCAD/EMTDC simulations of the LFO instability phenomenon.

As shown in Fig. 6(a), when the inner control gain of the dc–dc converter changes from initial parameters to improper parameters at 3 s, the dc-side voltage u_{dc} gradually diverges and its oscillation frequency is 12.50 Hz (the imaginary part of the mode is 78.54). The simulation in Fig. 6(a) is consistent with the root locus analysis in Fig. 5(a). Similarly, as shown in Fig. 6(b)–(d), when the other parameters fall into the improper range at 3 s, corresponding control components fall into instability. Therefore, the PSCAD/EMTDC simulations verify the effectiveness of root locus analysis.

4. Conclusion

In this paper, the LFO characteristics of the two-stage PV grid-connected system are analyzed based on the derived small-signal model, and the main conclusions are summarized as follows:

(1) There are LFO modes and HFO modes in the two-stage PV system. The LFO modes are dominated by the dc–dc converter, dc voltage control of dc–ac inverter, and the PLL control. The HFO modes are dominated by the dc-side LC circuit and ac-side LCL circuit. Compared with the HFO modes, the LFO modes present weaker damping and should be paid more focus.

(2) Improper control parameters setting of the dc–dc converter and dc–ac inverter can trigger LFO instability. The control gain of PLL and dc–dc converter inner loop should be kept small to maintain stability, whereas the dc-voltage outer control gain of dc–ac inverter should be kept large.

(3) The grid impedance has a different influence on the converter-dominated LFO mode and PLL-dominated LFO mode. The increase of grid impedance can suppress the converter-dominated LFO mode, and degrades the PLL-dominated LFO stability.

(4) Ignoring the dynamics of the dc–dc boost converter or assuming a constant dc-side voltage may result in a misleading conclusion, as the dc–dc converter and the dc voltage control of the dc–ac inverter greatly affect the LFO stability.

Declaration of competing interest

The authors declare that they have no known competing financial interests or personal relationships that could have appeared to influence the work reported in this paper.

Data availability

No data was used for the research described in the article.

Acknowledgments

References

[1] Li C. Unstable operation of photovoltaic inverter from field experiences. IEEE Trans Power Deliv 2018;33(2):1013–5.
[2] Morjaria M, Solar F. Experiences in deploying utility-scale PV power plants in weak grids. In: IEEE PES gen meeting. 2017.
[3] Zhao S, Li R, Gao B, Wang N, Zhang X. Subsynchronous oscillation of PV plants integrated to weak AC networks. IET Renew Power Gener 2019;13(3):409–17.
[4] Zhang M, Miao Z, Fan L. Reduced-order analytical models of grid-connected solar photovoltaic systems for low-frequency oscillation analysis. IEEE Trans Sustain Energy 2021;12(3):1662–71.
[5] Xia Y, Yu M, Wang X, Wei W. Describing function method based power oscillation analysis of LCL-filtered single-stage PV generators connected to weak grid. IEEE Trans Power Electron 2019;34(9):8724–38.
[6] Jia Q, Yan G, Cai Y, Li Y, Zhang J. Small-signal stability analysis of photovoltaic generation connected to weak AC grid. J Mod Power Syst Clean Energy 2019;7(5):1129–41.
[7] Zhao Z, Yang P, Wang Y, Xu Z, Guerrero JM. Dynamic characteristics analysis and stabilization of PV-based multiple microgrid clusters. IEEE Trans Smart Grid 2019;10(1):805–18.
[8] Shah R, Mithulananthan N, Lee KY. Large-scale PV plant with a robust controller considering power oscillation damping. IEEE Trans Energy Convers 2012;28(1):106–16.
[9] Eftekharnejad S, Vittal V, Heydy GT, Keel B, Loehr J. Small signal stability assessment of power systems with increased penetration of photovoltaic generation: a case study. IEEE Trans Sustain Energy 2013;4(4):960–7.
[10] Pukhrem S, Basu M, Conlon MF, Sunderland K. Enhanced network voltage management techniques under the proliferation of rooftop solar PV installation in low-voltage distribution network. IEEE J Emerg Sel Top Power Electron 2017;5(2):681–94.